International Journal of Nanomedicine

Dovepress

open access to scientific and medical research

Open Access Full Text Article

ORIGINAL RESEARCH

Remineralization of Dentin with Cerium Oxide and Its Potential Use for Root Canal Disinfection

Yinlin Wang[1], Xinyue Zhang[2], Haiyan Zheng[1], Zihuai Zhou[1], Si Li[1], Jimin Jiang[1], Mingxing Li[1], Baiping Fu[1]

[1]Stomatology Hospital, School of Stomatology, Zhejiang University School of Medicine, Clinical Research Center for Oral Diseases of Zhejiang Province, Key Laboratory of Oral Biomedical Research of Zhejiang Province, Cancer Center of Zhejiang University, Hangzhou, People's Republic of China; [2]School of Health Policy and Management, Chinese Academy of Medical Sciences & Peking Union Medical College, Beijing, People's Republic of China

Correspondence: Baiping Fu; Mingxing Li, Stomatology Hospital, School of Stomatology, Zhejiang University School of Medicine, Clinical Research Center for Oral Diseases of Zhejiang Province, Key Laboratory of Oral Biomedical Research of Zhejiang Province, Cancer Center of Zhejiang University, Hangzhou, People's Republic of China, Email fbp@zju.edu.cn; 7315019@zju.edu.cn

Objective: This study was to investigate a novel antibacterial biomimetic mineralization strategy for exploring its potential application for root canal disinfection when stabilized cerium oxide was used.

Material and Methods: A biomimetic mineralization solution (BMS) consisting of cerium nitrate and dextran was prepared. Single-layer collagen fibrils, collagen membranes, demineralized dentin, and root canal system were treated with the BMS for mineralization. The mineralized samples underwent comprehensive characterization using various techniques, including transmission electron microscopy (TEM), high-resolution TEM (HRTEM), Fourier transform infrared spectroscopy (FTIR), scanning transmission electron microscopy (STEM), selected-area electron diffraction (SAED), energy-dispersive X-ray spectroscopy (EDX), X-ray photoelectron spectroscopy (XPS), scanning electron microscopy (SEM), and micro-CT. Additionally, the antimicrobial properties of the BMS and the remineralized dentin were also analyzed with broth microdilution method, live/dead staining, and SEM.

Results: Cerium ions in the BMS underwent a transformation into cerium oxide nanoparticles, which were deposited in the inter- and intra-fibrillar collagen spaces through a meticulous bottom-up process. XPS analysis disclosed the presence of both Ce (III) and Ce (IV) of the generated cerium oxides. A comprehensive examination utilizing SEM and micro-CT identified the presence of cerium oxide nanoparticles deposited within the dentinal tubules and lateral canals of the root canal system. The BMS and remineralized dentin exhibited substantial antibacterial efficacy against E. faecalis, as substantiated by assessments involving the broth dilution method and live/dead staining technique. The SEM findings revealed the cell morphological changes of deceased E. faecalis.

Conclusion: This study successfully demonstrated antibacterial biomimetic mineralization as well as sealing dentinal tubules and lateral branches of root canals using cerium nitrate and dextran. This novel biomimetic mineralization could be used as an alternative strategy for root canal disinfection.

Keywords: cerium oxide, dextran, biomimetic mineralization, root canal disinfection

Introduction

Root canal treatment (RCT) is a widely recommended endodontic therapy for teeth with irreversible pulpitis and/or apical periodontitis.[1–3] The RCT procedure entails the thorough removal of the infection source from the root canal through a series of steps, including root canal preparation, irrigation, sealing, and precise obturation. However, achieving the goal of thoroughly cleansing the human tooth root canal system remains a significant challenge due to its complex internal anatomical structures, such as lateral canals, isthmuses or C-shaped canals.[4] Although dental procedures can reach the entire length of a root canal, some infectious sources can be left in some areas in which dental instruments and disinfectant solutions are inaccessible to.[5,6] When the apical-coronal seal is inadequate, tissue fluids rich in glycoproteins may permeate into the root canal, creating a favorable environment for the remaining microorganisms to thrive, leading to their proliferation and eventually resulting in the initiation or perpetuation of a periradicular lesion.[7] Indeed, despite

Received: 19 September 2023
Accepted: 12 December 2023
Published: 30 December 2023

the high success rate of endodontic treatment, root canal reinfections and their associated apical periodontitis lesions remain to be a great challenge.[8]

To address the limitations of mechanical and chemical preparations in root canal therapy, intracanal medicaments are frequently employed to further reduce bacterial presence.[9] Various intracanal medicaments, such as calcium hydroxide, iodine potassium iodide, eugenol, formocresol, phenolic compounds, and different antibiotics, have been widely suggested in dental history.[10] However, certain medicaments have fallen out of favor due to concerns regarding potential mutagenic and allergenic effects. Currently, calcium hydroxide remains the primary choice as an intracanal medicament for pulp necrosis with apical infections.[11] Numerous classic studies have demonstrated that calcium hydroxide possesses the ability to decrease bacterial load owing to its highly alkaline properties, tissue-dissolving capabilities, and antimicrobial properties.[12] Nevertheless, the effectiveness of calcium hydroxide has been questioned, particularly against bacteria such as E. faecalis, which is notorious for being difficult to eradicate and is frequently associated with recalcitrant root canal infections.[13,14] Calcium hydroxide also exhibits limited capacity to adequately disinfect dentinal tubules and has the potential to weaken the root structure if used for extended periods.[15]

In recent years, nanoparticle-based disinfection therapies have garnered significant interest within the endodontic research community. Among these, metal and metal oxide nanoparticles have been extensively investigated for their antibiofilm, antimicrobial, and antifungal properties in root canal disinfection strategies.[16,17] However, the use of nanoparticles may not offer long-term antimicrobial activity, leaving the possibility of reinfection with residual microorganisms over time.[10,18,19]

Cerium oxide nanoparticles have attracted considerable attention as a promising material due to their potent antibacterial and anti-inflammatory properties.[20] These nanoparticles possess a unique surface composition comprising Ce (III), Ce (IV), and oxygen vacancies, which grants cerium oxide dual redox capabilities. Extensive research has substantiated the ability of cerium oxide nanoparticles to impede the growth of various bacteria, such as E. faecalis and S. mutans[21,22] while demonstrating excellent biocompatibility.[23] However, if cerium oxide nanoparticles are directly used for root canal disinfection, they may still not provide long-lasting antibacterial effects, similar to other metal nanoparticles.

Biomimetic mineralization is a process that imitates natural biomineralization by replacing the water in the demineralized organic matrix with apatite crystallites, which is a powerful approach to synthesizing advanced materials with specific structures and functions.[24,25] This strategy has already found applications in sealing dentinal tubules and restoring the mechanical strength of root dentin using hydroxyapatite in the field of root canal treatment.[26,27] If nano cerium oxide deposits within the collagen fibrils of demineralized dentin via biomimetic mineralization, it can not only effectively seal areas that are inaccessible to using both mechanical and chemical methods but also address any residual bacteria. Additionally, the remineralized dentin could continuously release antibacterial components for long-term antibacterial purposes.

The objective of this study was to explore a novel dentin biomineralization scheme for integrating stabilized cerium oxide into collagen fibrils and investigating its potential application for root canal disinfection. The null hypotheses tested were as follows: 1) Demineralized dentin cannot be remineralized with cerium oxide; 2) Dentin tubules and lateral canals cannot be occluded by cerium oxide using the principle of biomimetic remineralization; 3) Dextran-stabilized cerium oxide and the surface of cerium oxide-remineralized dentin have no antibacterial activity against E. faecalis.

Materials and Methods

Preparation of Biomimetic Mineralization Solution (BMS)

Dextran (Mw: 40 kDa, Shanghai Macklin Biochemical Co., China) was dissolved in deionized water to form a homogeneous solution, and then $Ce(NO_3)_4$ (Shanghai Macklin Biochemical Co., China) powder was added slowly under magnetic stirring. After the powder was completely dissolved, the pH value of the solution was adjusted to 7.0 with 1 M NaOH to form a biomimetic mineralization solution (BMS). The final concentration of each component in the solution was 1g/mL dextran, 4.5 mM $Ce(NO_3)_4$.

Mineralization and Characterization of Single-Layer Collagen Fibrils

A single-layer collagen model was prepared following our laboratory protocol.[28] Initially, a drop of rat tail type I collagen stock solution (3 mg/mL, Gibco Invitrogen, USA) was diluted in 0.5 mL of buffer solution (50 mM glycine, 200 mM KCl, pH=9.2). After being kept at room temperature for 20 min, a 5 μL drop of the collagen solution was applied onto a carbon-and-formvar-coated nickel grid. The grid was then incubated in a 100% humidity chamber at 37°C for 8 h. Subsequently, the grid was treated with 0.05 wt% glutaraldehyde solution for 1 h to facilitate collagen cross-linking, rinsed with deionized water and air-dried.

The collagen-coated grids (n=24) were placed upside down, floating on 10 mL of BMS at 37°C during the incubation period. After 0 (control), 3, 7, and 14 d, the grids (n=6) were meticulously retrieved and gently washed with deionized water. Subsequently, they were sequentially dehydrated using an aqueous ethanol solution (50 v/v%) followed by anhydrous ethanol. The samples were then analyzed using transmission scanning microscopy (TEM, JEM-1400 TEM, JEOL, Japan) and high-resolution TEM (HRTEM, FEI Tecnai G2 F20 S-TWIN, FEI, USA) incorporating selected area electron diffraction (SAED) and energy dispersive X-ray analysis (EDX, Oxford. X-MAX 80T).

Mineralization and Characterization of Collagen Membranes

Thirty-six collagen membranes (5 × 5 mm), cut from Bio- Gide® collagen membrane (BG; Geistlich, Wolhusen, Switzerland), were fixed with 2.5% glutaraldehyde for 2 h and thoroughly rinsed with deionized water. Then, they were incubated in 10 mL of the BMS at 37°C for 0 (control), 7 or 14 d (n=12 for each group) before being collected for characterization.

Three collagen membranes from each group were fixed in 2.5% glutaraldehyde, dehydrated in an ascending series of ethanol solutions (30–100 v/v%), immersed in propylene oxide and embedded in epoxy resin. The collagen membranes were prepared into ultrathin sections with 70–90 nm of thickness without further staining using an ultramicrotome (EM UC6, Leica, Germany) and examined using TEM (JEM-1230, JEOL, Tokyo, Japan).

Six collagen membranes from each group were placed in a vacuum vessel for complete drying. The mineralized and unmineralized collagen membrane samples were elucidated using an attenuated total reflectance Fourier transform infrared (ATR-FTIR) spectrophotometer (Thermo Fisher Scientific, USA). Infrared spectra were obtained by performing 50 scans within the range of 4000–400 cm^{-1}, with a resolution of 4 cm^{-1}.

Three collagen membranes from each group underwent analysis through X-ray photoelectron spectroscopy (XPS) using an ESCALAB 250Xi instrument (Thermo Fisher Scientific, USA). The XPS analysis utilized Al Kα radiation as the monochromatic source and employed an irradiated region spot diameter of 500 μm. The measured binding energy of C1s was 284.8 eV. All spectral processing was performed using OriginPro 9.3 software (Origin Laboratory Corp., USA).

Remineralization and Characterization of Dentin

The study was conducted in accordance with the 1964 declaration of HELSINKI and later amendments. A total of 60 non-caries human third molars were obtained with written informed consent. The protocol was approved by the Institutional Ethics Committee of Zhejiang University School of Stomatology (Approval number: #2018017). The teeth were stored in 0.5% chloramine T solution at 4°C and used within 1 month after extraction.

Thirty-six dentin disks with a thickness of 1 mm were prepared using a low-speed Isomet saw (Buehler Ltd., Lake Bluff, IL, USA) with water cooling. To achieve a flat dentin surface, the disks were sequentially polished with #600-, 1200-, 3000- grit silicon carbide papers in a polishing machine (ATM Saphir 360, Germany) under running water. The polished surfaces of the dentin disks were conditioned with 17% ethylenediaminetetraacetic acid (EDTA) for 2 min and rinsed with water for 30s. These conditioned dentin disks were sequentially incubated in 10 mL BMS at 37°C for 0 (control), 7 and 14 d (n=12 for each group). Following the remineralization process, the dentin disks were thoroughly rinsed with deionized water to remove the loosely bound minerals from the dentin surfaces.

Twelve dentin disks from each group were examined using TEM, scanning electron microscopy (SEM, HITACHI, SU8010, Tokyo, Japan) and ATR-FTIR (n=4 for each item).

Remineralization and Micro-CT Analysis of the Root Canals

Root Canal Preparation and Remineralization

Six extracted human premolars were selected for this study. The access cavities were prepared through the crown using an endo access bur (EX-41, Dia burs-MANI Inc, Tochigi-Ken, Japan), which was prepared with a high-speed handpiece equipped with an air-water spray. The pulp tissues were carefully extirpated, and the working length of the canals was determined. During the cleansing and shaping of root canals, apical enlargement was carried out until #25K-files were used. Subsequently, ProTaper files (#F1, F2, F3, Dentsply-Maillefer, Ballaigues, Switzerland) were used to cleans and shape the root canals according to the technique described by Yared.[29] To ensure effective cleansing, the irrigation was done with 3% sodium hypochlorite (Longly Biotechnology, Wuhan, China). The smear layer formed during the root canal preparation was removed by treating the canal surface with 17% EDTA for 2 minutes. Then, teeth with root canals prepared were each immersed in 10 mL of BMS at 37°C for 14 d for remineralization.

Micro-CT Scanning

The above-mentioned teeth with prepared root canals were scanned both before and after remineralization using a bench-top micro-CT scanner (Milabs, Netherlands) to observe the deposition of cerium oxide within the root canal system. To achieve optimal image quality, the X-ray tube voltage and current were set at 850kV and 210 μA, respectively, with a resolution of 75 μm. The data obtained were subjected to 3D reconstruction using Milabs 3D Reconstruction software, employing an isotropic volumetric pixel (voxel) size of 10 μm. The resulting 3D image data were then examined and processed using Imalytics Preclinical 2.1 (Version 2.1.8.9).

Evaluation of Antimicrobial Properties

Planktonic Bacteria

E. faecalis strain ATCC 29212 (Beijing Baocang Biotechnological Co., Ltd., China) was reactivated from the stock cultures in brain heart infusion broth (BHI, BD Biosciences, Bergen, NJ, USA) at 37°C for 24 hours and then subcultured in brain heart infusion agar plates and incubated at 37°C for another 24 hours. A single colony was selected from brain heart infusion agar plates and incubated in BHI broth for 24 hours to make bacteria proliferate. Subsequently, the bacteria were diluted with fresh BHI to achieve a final concentration equivalent to 0.5 McFarland standard using a nephelometer. (Thermo Fisher Scientific, USA).

The minimum inhibitory concentration (MIC) was employed to assess the antibacterial activity of the BMS against planktonic E. faecalis by the broth microdilution method. To initiate the assay, 100 μL of fresh BHI was added to each well of a 96-well plate, after which 100 μL of cerium nitrate and dextran solution, twice the concentration of BMS, was added to the first well. The contents were thoroughly mixed, and then 100 μL of the mixture from the first well was transferred to the next well, resulting in a 50% reduction in concentration. This process was repeated 6 times to establish a range of concentrations. Next, 100 μL of a diluted bacterial suspension was added to each well, and the plate was placed in an incubator at 37 °C for 24 hours. The bacterial activity was measured by recording the optical density (OD) at 600 nm using a microplate reader (SpectraMax i3, Molecular Devices, China). To serve as growth controls, wells containing medium with inoculums but without the BMS were also included in the assay. Each group was performed in sextuplicate to ensure the accuracy and reliability of the results.

Direct Contact Test

The direct contact test (DCT) was performed to evaluate the antibacterial activity of remineralized dentin surface with a LIVE/DEAD BacLight Bacterial Viability Kit (L7012, Thermo Fisher Scientific, Waltham, MA, USA) containing SYTO 9 green-fluorescent nucleic acid stain and propidium iodide, the red-fluorescent nucleic acid stain.[30,31] The following surfaces were tested: (i) polished dentin surfaces without remineralization (control, n = 3), (ii) 14-day remineralized dentin surfaces (n=3). All the samples underwent sterilization under ultraviolet light for 4 h before utilization. A volume of 10 μL of standardized bacterial suspension was placed on the surface of each sample and incubated at 37°C for 1 hour. Once the suspension liquid evaporated, ensuring direct contact between the bacteria and the dentin surface, 300 μL of BHI was added to each well. The samples were then incubated anaerobically at 37°C for 24

hours. After incubation, the dentin samples were stained with 6 μM SYTO 9 and 30 μM propidium iodide as per the manufacturer's instructions. Subsequently, they were examined using a confocal laser scanning microscope (CLSM, Leica SP8, Germany). The channels were set at 488 nm for live bacteria (SYTO 9; green fluorescence) and 552 nm for dead bacteria (propidium iodide; red fluorescence). From each disk, five locations were randomly selected for image acquisition, resulting in a total of 15 locations analyzed. The percentage of dead bacteria within the biovolume of each sample surface was analyzed using ImageJ software (Version 1.53k, National Institutes of Health, USA).

Scanning Electron Microscope (SEM) Observation

Scanning electron microscope (SEM) was employed to observe the bacterial morphology on the tested samples. The bacteria were cultivated on the dentin surfaces following the previously described procedures (n = 9 for each group). Subsequently, the tested dentin surfaces were gently washed with PBS and then fixed with 2.5% glutaraldehyde using an ascending series of ethanol solutions (50%, 70%, 85%, 90%, and 100%) for 15 minutes each. After the dehydration process, the samples were dried and sputter-coated with gold nanoparticles using an ion-sputter coater for 10 seconds. Observations were carried out under an SEM(HITACHI, SU8010, Tokyo, Japan) at 3 kV.

Statistical Analyses

Data analyses were performed using SPSS version 26 (SPSS, Chicago, Illinois, USA). Data sets derived from each experiment were first evaluated for their normality and homoscedasticity assumptions prior to the use of parametric statistical methods. Independent sample *t*-test were used to evaluate the antibacterial effect of the BMS and the remineralized dentin surfaces.

Results

Mineralization and Characterization of Single-Layer Collagen Fibrils

After immersion in BMS, Ce-collagen fibrils exhibited progressive mineralization over time, and periodic transverse lines of 67 nm were observed on the surface of Ce-collagen fibrils after incubation for 3 d (Figure 1a). A large number of small, diffusely distributed crystals were visible around the collagen fibrils, and significant mineralization was detected within the collagen fibrils after 7 d. (Figure 1b). After 14 d of incubation, the collagen fibrils had been heavily mineralized, and the electron density of fibrils was extremely high (Figure 1c). HRTEM analysis showed that intrafibrillar mineralization with Ce-collagen fibril after 14 d (Figure 1d). The SAED pattern (Figure 1e) unraveled that the mineral form within the mineralized collagen fibrils was cerium oxide, which revealed typical 111, 220 and 311 diffraction rings.[25] The lattice spacing of the crystals deposited on the Ce-collagen fibril was found to be 3.19 Å, matching that of cerium oxide[32] (Figure 1f). Moreover, the elemental mapping results (Figure 1g) demonstrated that the mineral crystals within the Ce-collagen fibril contained an abundance of cerium and oxygen elements.

Mineralization and Characterization of Collagen Membranes

With the treatment of BMS, dense minerals were deposited within the collagen membranes. HRTEM imaging showed the typical interplanar spacing: 3.19 Å, which was found to be consistent with cerium oxide. The SAED pattern also confirmed that the mineral formed within the collagen fibrils was cerium oxide. The FTIR spectra for the pure membrane, CeO_2 nanoparticles, and Ce-collagen membranes were presented in Figure 2d. In the spectrum of the pure collagen membrane, prominent transmittance peaks corresponding to the four principal amide groups are evident.[33] Specifically, peaks located at approximately ~1640, ~1545, and ~1240 cm^{-1} correspond to the amide I (C═O stretch), amide II (NH bend coupled with CN stretch), and amide III (NH bend coupled with CN stretch) vibrations of collagen, respectively. Additional peaks at ~3300 and ~2920 cm^{-1} are attributed to the amide A (NH stretch coupled with hydrogen bond) and amide B (CH2 asymmetrical stretch) bands.[34] The appearance of peaks at ~3388 and ~1618 cm^{-1} indicates the stretching and bending vibrations of the -OH group. Moreover, peaks at ~1382 and ~690 cm^{-1} signify the stretching and bending vibrations of Ce-O-Ce bonds.[35,36] Notably, distinct new peaks at ~690 cm^{-1}, consistent with CeO_2 nanoparticles, were discernible in the FTIR spectra of Ce-collagen membranes. Furthermore, an intriguing observation was the shift of the amide III vibration of the membranes (initially at ~1240 cm^{-1}) to a peak at ~1230 cm^{-1} because of the in-plane bending

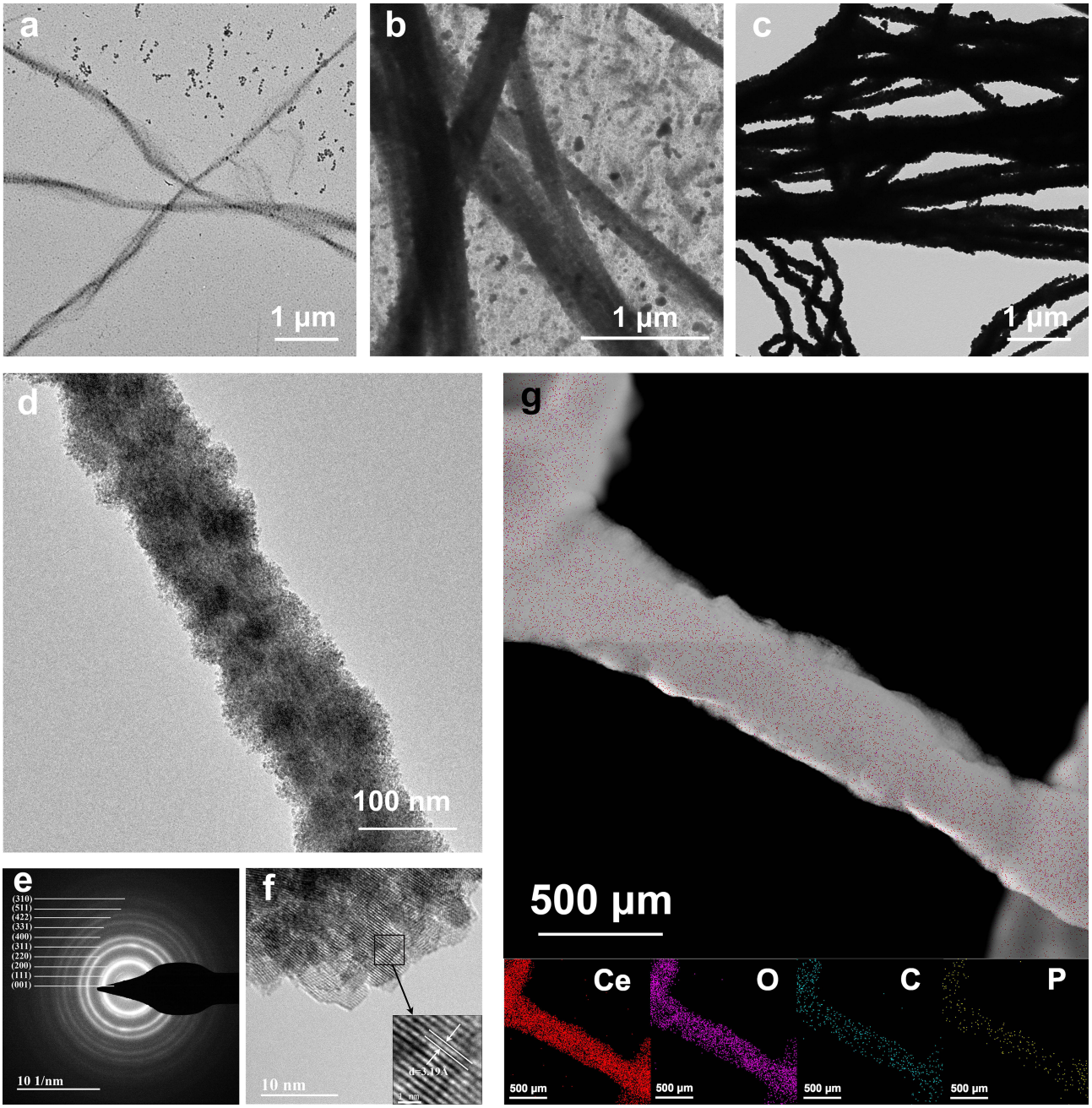

Figure 1 TEM, HRTEM, STEM, and mapping images of collagen fibrils treated with BMS. (**a**) TEM image of Ce-collagen fibrils after incubation for 3 d, revealing high electron density. (**b**) After 7 d of incubation, mineral deposition within collagen fibrils could be observed. (**c**) Dense minerals deposited within Ce-collagen fibrils after 14 d. (**d**) HRTEM image reveals intrafibrillar mineralization after 14 d. (**e**) The SEAD pattern unravels the mineral form within the Ce-collagen fibrils with 111, 220 and 311 diffraction rings. (**f**) HRTEM image shows the typical interplanar spacing: 3.19 Å. (**g**) The STEM image of the mineralized collagen and elemental mapping reveals the even distribution of the elements. The scale bars for each figure are located at the corner of the panels.

of C–N and N–H.[37] Furthermore, XPS imaging of collagen membranes after 7 and 14 d of incubation showed the presence of cerium, and the ratio of Ce (IV) to Ce (III) was 54.12%: 45.88% (7 d) and 74.7%: 25.3% (14 d) respectively.

Remineralization and Characterization of Dentin

After the dentin surface was treated with 17% EDTA for 2 min, a demineralization depth of approximately 0.8 μm was visible (Figure 3a). After 7 and 14 d of mineralization, the previously demineralized part had been completely mineralized (Figure 3b, and c). The STEM image and elemental mapping results (Figure 3d) showed an abundance of

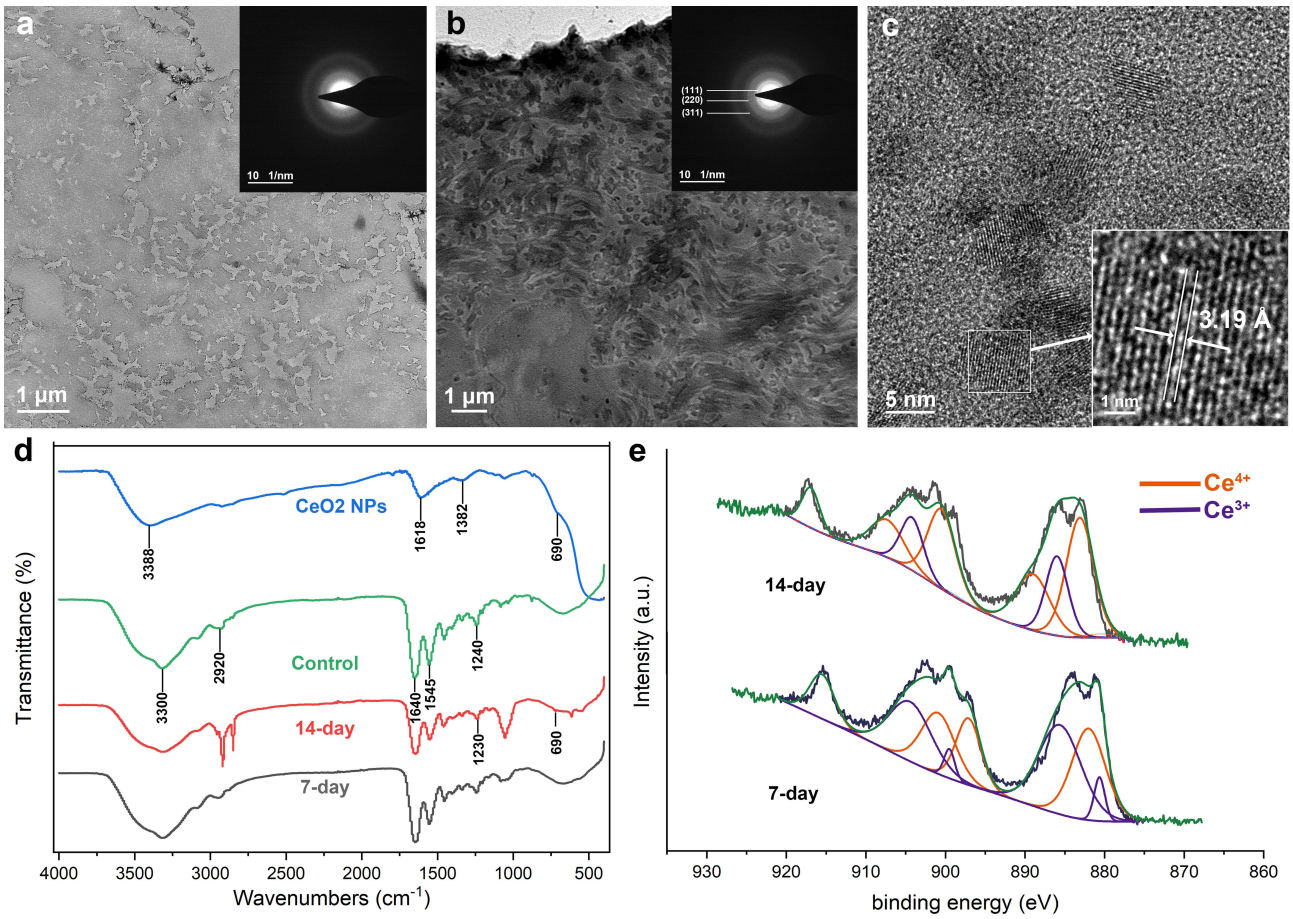

Figure 2 TEM, HRTEM, FTIR and XPS images of collagen membranes treated with BMS. (**a**) TEM image of pure collagen membranes reveals low electron density, while the inset SAED image shows the amorphous state. (**b**) Dense minerals were deposited within Ce-collagen fibrils after 14 d, with the SAED pattern unraveling the mineral form within the collagen fibrils (inset). (**c**) HRTEM image that reveals the crystal spacing of crystals within collagen. (**d**) FTIR spectra of Ce-collagen membranes after incubation for 14 d demonstrate that the mineralized crystals are identical to cerium oxide. (**e**) The XPS images of Ce-collagen membranes after incubation for 7 and 14 d. The scale bars are marked in the corner of the panels.

cerium and oxygen elements in the remineralized dentin. SEM analysis revealed a substantial accumulation of mineral deposits on the remineralized dentin surface, resulting in partial obstruction of the dentin tubules (Figure 3e and f). In the control group, the FTIR spectra of demineralized dentin showed that the peaks at ~3300, ~1640, ~1545 and ~1240 cm^{-1} were assigned to amide A, I, II and III bands[34,38] (Figure 3g). Whereas the FTIR spectra of the remineralized dentin exhibited new peak appeared at ~ 690 cm^{-1} which was derived from CeO_2 nanoparticles. The peak at ~1545 cm^{-1} of amide II was shifted to ~1490 cm^{-1} which was associated with C=O stretching, and the peak at ~1640 cm^{-1} of amide I was shifted to ~1630 cm^{-1} which was associated with N–H bending and C–N stretching.[37] These were caused by the incorporation of cerium oxide in the mineralizing dentin. XPS analysis of dentin surface (Figure 3h) mineralized for 7 and 14 d showed that the ratio of tetravalent to trivalent cerium was 30.4%:69.6% for 7-day mineralized samples and 62.28%:37.72% for 14-day samples.

Remineralization and Micro-CT Analysis of the Root Canals

Representative micro-CT images before and after remineralization were presented in Figure 4. The micro-CT images of the longitudinal and cross-sectional interfaces of a tooth after the root canal was treated with 17% EDTA (Figure 4a and b). At baseline, the root canal dentin wall appears less dense than elsewhere in the tooth. On the other hand, after 14 d of incubation, a clearly uniform layer of high-density mineralized deposition was visible in the root canal dentin wall (Figure 4c and d). Figure 4e reveals that the density of the remineralized crystal deposit layer on the inner wall of the

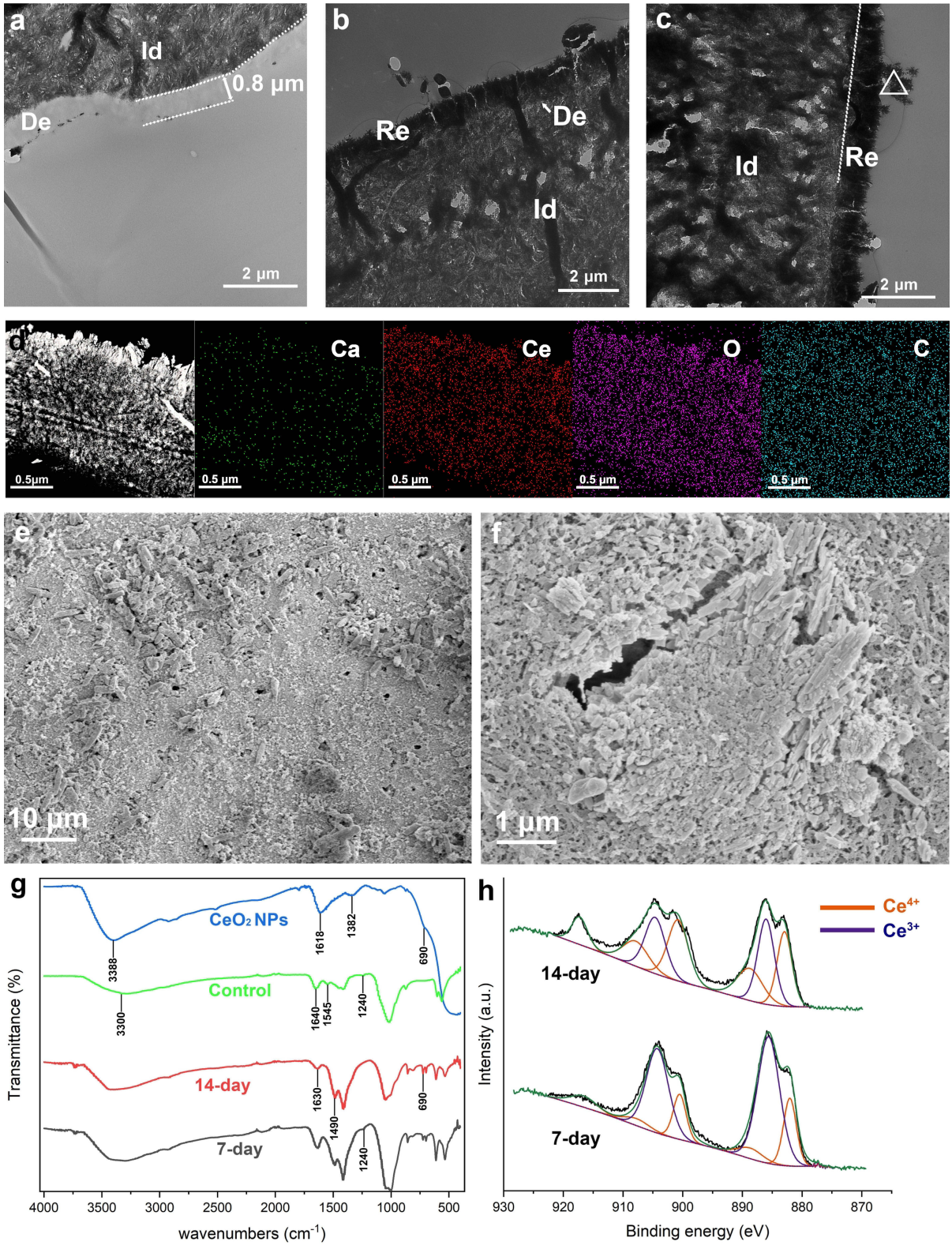

Figure 3 TEM, STEM, mapping, SEM, FTIR, and XPS images of dentin treated with BMS. "Re" marked in the panels represents the remineralized dentin, "De" represents demineralized dentin, and "Id" represents intact dentin. Δ represents the crystals deposited in dentinal tubules and dentin surfaces. (**a**) The TEM image shows demineralized dentin resulting from treatment with 17% EDTA. (**b** and **c**) The TEM image shows dentin treated with BMS for 7 d (**b**) and 14 d (**c**). (**d**) The STEM image and elemental mapping revealed the even distribution of the elements after the demineralized dentin was treated with 17% EDTA and subsequently incubated after 14 days. (**e** and **f**) The SEM images of the surface of remineralized dentin. (**g**) The ATR-FTIR image demonstrates that the mineralized crystals are identical to cerium oxide. (**h**) The XPS images of 7- and 14-day remineralized dentin. The scale bars are marked in the corner of the panels.

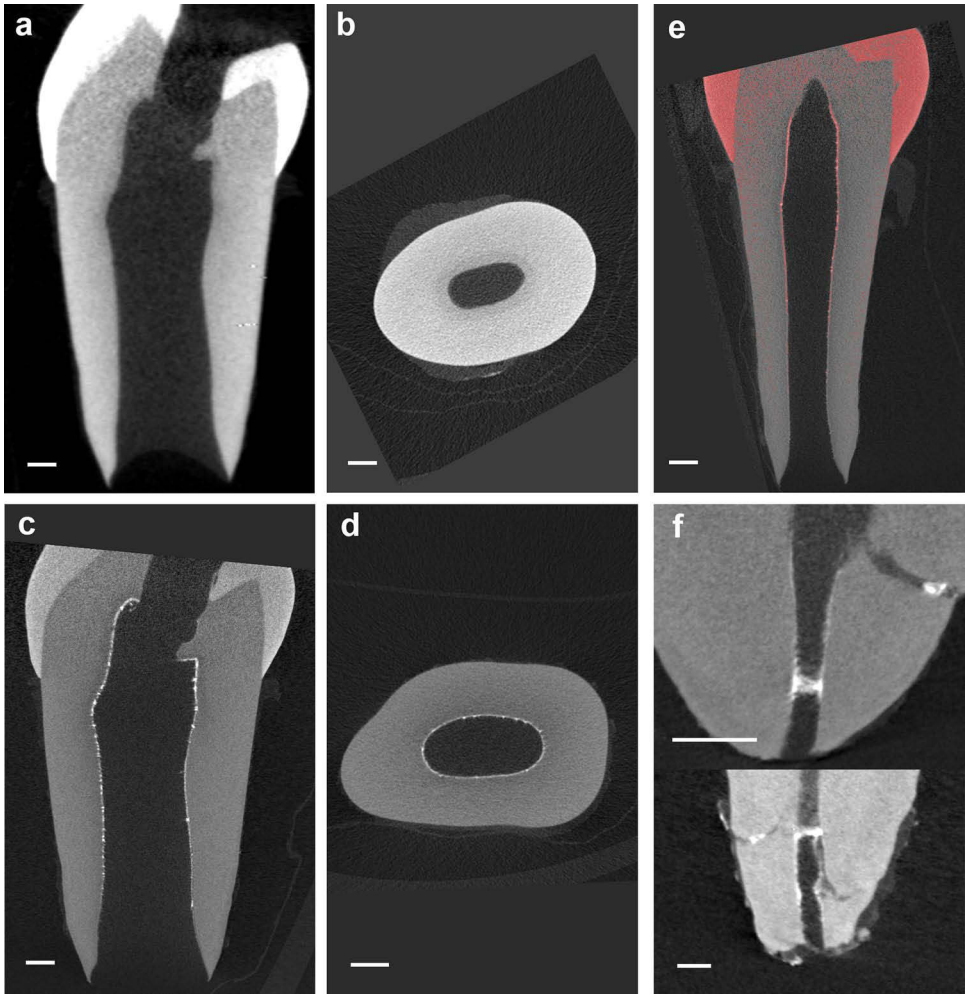

Figure 4 Micro-CT images of root canals treated with EDTA during root canal preparation are presented in (**a** and **b**), displaying the longitudinal and cross-sectional sections, respectively. (**c** and **d**) show the corresponding images of remineralized root canals. The high-density range of micro-CT images (gray values distributed above 7000) is highlighted in red (**e**). The density of the remineralized crystal deposit layer on the inner wall of the root canal was higher than natural root canal. (**f**) High-density mineral deposits can also be observed in the lateral root canals of the teeth. Scale bar: 1 mm.

root canal was higher. Figure 4f shows that cerium oxide can be effectively deposited within the lateral root canals through remineralization.

Evaluation of Antimicrobial Properties

Minimum Inhibitory Concentration (MIC)

As shown in Figure 5, when dextran, cerium nitrate, and dextran-cerium nitrate were diluted to 1/8($3.12*10^{-3}$ mM), 1/2 (2.25 mM), and 1/32 ($7.80*10^{-7}$ mM, 0.14 mM) of the original concentration, there were significant differences of optical density compared with the control group. Therefore, the MIC results revealed that the MIC of dextran against E. faecalis was $3.12*10^{-3}$ mM, the MIC of cerium nitrate against E. faecalis was 2.25mM, and the MIC of BMS, ie dextran+cerium nitrate against E. faecalis, was $7.80*10^{-7}$ mM-0.14 mM.

Direct Contact Test

Figure 6a depicts a confocal fluorescence image of E. faecalis, stained with the staining kit, to distinguish between live and dead bacteria. The fluorescence images were obtained under excitation at 488 and 552 nm, respectively. The image shows the mixed population of live and dead bacteria in the control group, where untreated dentin exhibited a high abundance of live Enterococcus faecalis with only a few dead bacteria after 24 hours of incubation. Conversely, after 24 hours of incubation, a large number of dead bacteria and a small amount of live bacteria were observed on the surface of

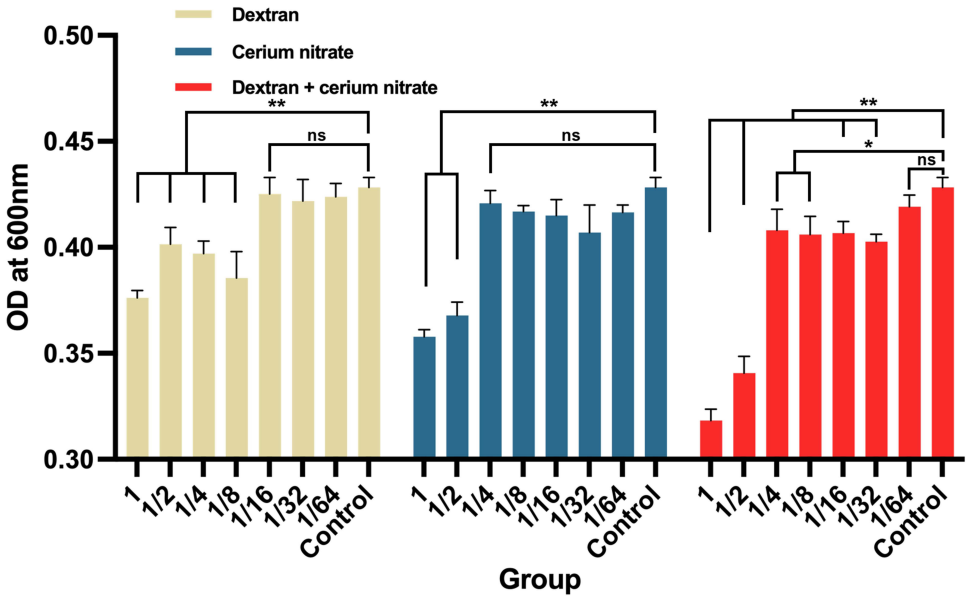

Figure 5 Optical density of bacterial fluid after adding different concentrations of dextran, cerium nitrate or dextran-cerium nitrate. All data are presented as Mean±S.D. **P<0.01 vs the control group; *P<0.05 vs the control group; ns, not significant.

remineralized dentin. As depicted in Figure 6b, a significant disparity was observed in the number of live and dead bacteria between the control group and the remineralized group (P<0.001). Additionally, a statistically significant difference was noted in the ratio of live/dead bacteria between the control group and the 14-day group (P<0.05).

Scanning Electron Microscope (SEM) Observation

The morphology of E. faecalis bacteria on the dentin surface was examined using SEM, as shown in Figure 7. In the control group, a substantial number of intact E. faecalis bacteria were observed attached to the dentin surface, with visible bacterial divisions. Conversely, the cerium remineralized group exhibited a decrease in bacterial viability, as evidenced by the presence of dead bacteria on the dentin surface (Figure 7a and b). Ruptured bacterial envelopes and the absence of intramembranous organelles and cell fluid were observed (as shown by the white arrow). Some abnormal bulges on the bacterial cell membrane could be seen (Figure 7c and d).

Discussion

The complete eradication of microorganisms in the root canal system is essential for the long-term success of root canal therapy.[39] However, the existing mechanical and chemical techniques often failed to achieve optimal outcomes.[16,40] Consequently, numerous researchers have explored the use of novel materials to achieve full sealing and sustained antibacterial effects,[16] among which metal oxide nanoparticles in root canal disinfection have been extensively investigated.[17,41,42] However, when incorporated into root canal disinfection, the antibacterial efficacy of nanoparticles is typically confined to the main root canal surface and may not adequately reach intricate anatomical structures like lateral canals and dentin tubules, and often lack persistence.[43–45] This study employed a biomimetic mineralization strategy to synthesize cerium oxide nanoparticles in situ on demineralized dentin surfaces. These nanoparticles, embedded in demineralized dentin, will not be released in large quantities in a short time. This theoretically benefits a sustained antibacterial effect over time. Moreover, they possess the ability to effectively seal minor cavities, encompassing lateral root canals and dentin tubules, presenting a promising solution to address the concern of microbial residue in infected root canals. In light of this, we employ cerium nitrate as a raw material in our endeavor to develop intracanal medication with antibacterial properties and biomimetic mineralization potential.

A single-layer of type I collagen fibrils is a convenient model for the rapid screening of biomimetic mineralization formulations.[46,47] In the current experiment, TEM images reveal that with the extension of mineralization time, the

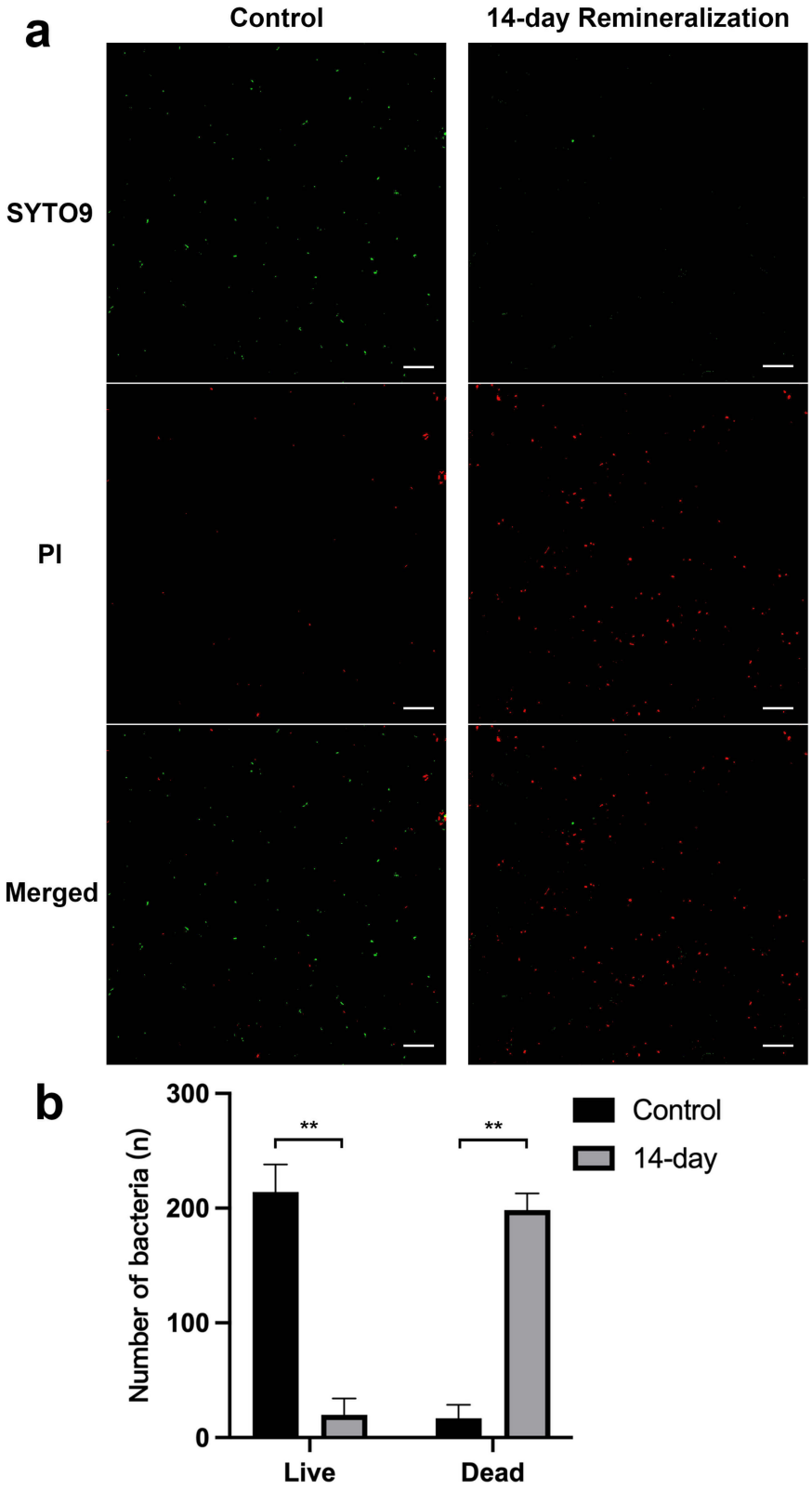

Figure 6 (**a**) Representative fluorescence micrographs and count of live/dead E. faecalis in the control group and the remineralized dentin group. The green dots correspond to live E. faecalis, and the red dots indicate dead E. faecalis. Scale Bar: 100 μm. (**b**) The average number of live/dead bacteria in each selected area of the control group and 14-day remineralized group. All data are presented as Mean±S.D. **P<0.01 vs the control group.

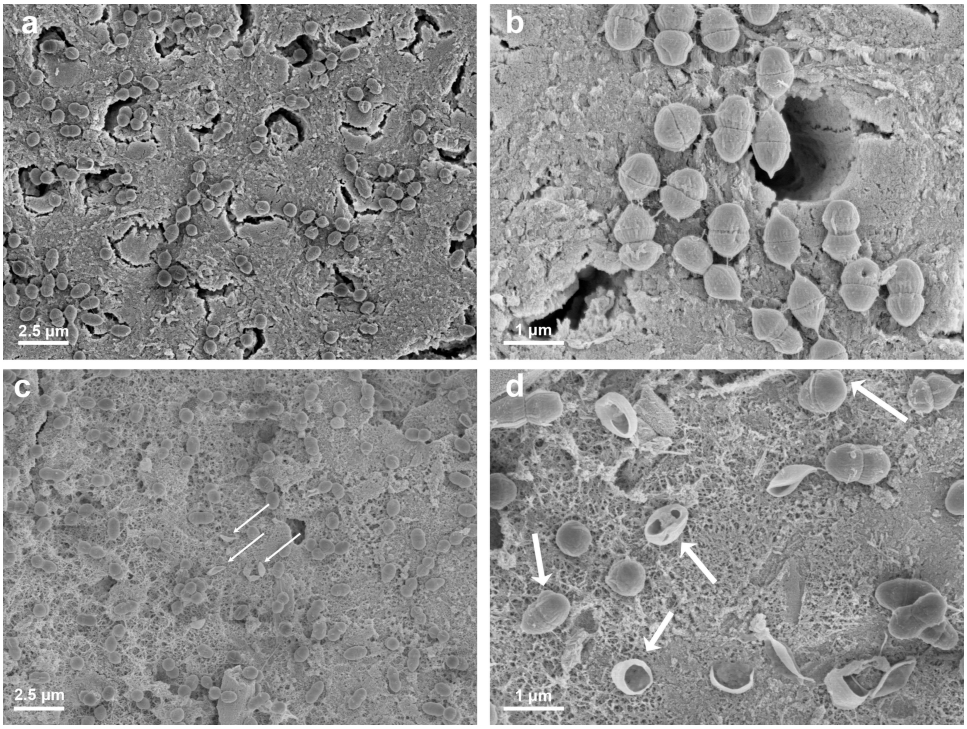

Figure 7 The morphology of Enterococcus faecalis on the surface of untreated dentin (**a** and **b**) and remineralized dentin (**c** and **d**) was examined using SEM. (**a** and **b**) The SEM images depict the approximate number and morphology of E. faecalis on the untreated dentin surface. (**c** and **d**) The morphology of E. faecalis on the surface of the remineralized dentin. The white arrows indicate abnormal bulges on the bacterial cell membrane and the ruptured bacterial envelopes.

single-layer collagen fibrils underwent a progressive and organized mineralization process. XPS analysis suggests that the mineralized material contains cerium oxide crystals. When cerium nitrate ($Ce(NO_3)_4$) is dissolved in water, it dissociates into cerium ions (Ce^{4+}) and nitrate ions (NO_3^-).[48] The cerium ions can undergo hydrolysis reactions in the presence of water to form cerium oxide.[49] The formation of cerium oxide in water is often accompanied by the release of heat, and the resulting cerium oxide particles may agglomerate and form larger particles or clusters because of their high surface energy.[49] To stabilize the dispersion of nanoparticles, surface modification, addition of dispersants or control of solution pH are often used to reduce agglomeration.[50,51] In this study, dextran was used to wrap and stabilize the state of cerium oxide nanoparticles. TEM analysis demonstrated the persistent presence of numerous dispersed nanoparticles in the solution even after 3 and 7 d of incubation (Figure 1a and b). This observation confirmed the effective stabilization of nano cerium oxide by dextran, aligning with the previous study.[32]

As the TEM analysis of the three-dimensional collagen membrane and demineralized dentin confirmed the occurrence of inter- and intra-fibrillar mineralization (Figures 2a-c; 3b and c), the null hypothesis that demineralized dentin cannot be remineralized with cerium oxide was rejected. Intra-fibrillar mineralization constitutes a crucial aspect of dentin biomimetic mineralization, wherein non-collagenous components and their analogs play a vital role in this process. They facilitate the formation of mineralized precursors and maintain their amorphous nature.[52] By leveraging capillary action, electrostatic attraction, and osmotic pressure, these amorphous precursors permeate the collagen fibers, leading to the orchestrated deposition of hydroxyapatite.[53] Dextran was selected as the non-collagenous analog for this particular experiment as it has a long chain structure and lots of hydroxyl groups.[54] The long chains are intertwined in the solution, which forms cross-linked spatial network structures through van der Waals forces or hydrogen bonding.[54–58] The network structures can restrict the metal cations while the functional hydroxyl groups can bind the metal cations, and both affect their crystallization.[55–58] Thus, it is speculated that the dextran bonded free cerium ions in the solution combined with oxygen in water, forming nano cerium oxide liquid-like precursors,[32,59] which can penetrate the gaps of the collagen fibrils and subsequently undergo transformation into cerium oxide crystals and deposited within the fibrils.[60]

The results from infrared spectroscopy unequivocally validated the substantial presence of cerium oxide within both the mineralized collagen film and the remineralized dentin. Notably, the observed red shift of the amide bonds strongly suggests a chemical adsorption phenomenon occurring between the mineralized substance and collagen molecules, further solidifying this interaction.[61] Furthermore, the chemical states of the mineralized collagen membrane and dentin measured using the XPS analysis revealed the presence of both Ce (III) and Ce (IV) redox states, and the proportion of Ce (IV) in the mineralization increased with the extension of immersion time notably (Figures 2d and e; 3g and h). The proportion of Ce (IV) in cerium oxide can be influenced by various factors, including the synthesis method, processing conditions, and subsequent exposure to different environments.[62] In the present study, one possible reason for the reduction of the Ce (III) /Ce (IV) ratio over time may be the interaction of the cerium oxide nanoparticle with the surrounding environment, such as oxygen, water, or other reactive species, which leads to the oxidation of the nanoparticle and the conversion of Ce (III) to Ce (IV).[22] Another potential factor is the agglomeration of the nanoparticle over time, as the Ce(III)/Ce(IV) ratio is negatively correlated to the particle size of cerium oxide nanoparticles.[63,64] The content of Ce (III) in nanoparticles is often associated with their antioxidant properties, while the content of Ce (IV) is linked to their antibacterial properties. Specifically, a higher proportion of Ce(IV) in cerium oxide nanoparticles tends to significantly enhance their antibacterial properties.[22] However, it is important to note that the balance between Ce (III) and Ce (IV) ions in cerium oxide nanoparticles can be critical for achieving optimal antioxidant and antibacterial properties.[22,65] To determine the optimal ratio for intracanal medication, future experiments should aim to evaluate the antibacterial efficacy and cytotoxicity of different Ce (III) /Ce (IV) ratios against the target bacteria.

Bacteria have the ability to survive under low oxygen tension and nutrient-deprived conditions by forming biofilms, which can adhere to different areas within the root canal system, including dentinal tubules, lateral canals, and periapical regions.[66] Biomineralization processes, such as the deposition of hydroxyapatite crystals, can help seal and occlude dentinal tubules.[26,67,68] This sealing effect prevents the re-entry of bacteria and their byproducts into the root canal system, reducing the risk of reinfection and enhancing the effectiveness of disinfection protocols.[69,70] In this experiment, SEM analysis revealed varying degrees of closure in the majority of dentinal tubules following dentin mineralization. The micro-CT images exhibited a dense layer of mineral deposition, effectively covering the inner wall of the root canal, with evident sealing observed in the lateral root canal and apical foramen. These outcomes promote comprehensive disinfection of the root canal, enhancing the efficacy of the procedure. Thus, the null hypothesis that dentin tubules and lateral canals cannot be occluded by cerium oxide using the principle of biomimetic remineralization was rejected.

In addition to these indirect disinfection effects, the live/dead bacterial staining results confirmed that both the intracanal medication and the mineralized dentin surface had a good bactericidal effect. Thus, the null hypothesis that dextran-stabilized cerium oxide and the surface of cerium oxide-remineralized dentin have no antibacterial activity against E. faecalis was rejected. Unlike other antibacterial bioactive materials recognized for their mineralization potential and reliance on cation release, cerium oxide nanoparticles, which are positively charged, can adsorb onto negatively charged Gram-positive and Gram-negative bacteria through electrostatic interaction.[71,72] They can also inflict direct damage to the cell membranes because of the irregular shapes and rough edges,[73,74] induce oxidative stress,[75,76] and interfere with nutrient transport,[77,78] leading to bacterial death. When cerium oxide nanoparticles are adsorbed onto the surface of bacterial membrane, they can combine with intermediates and interfere with cellular respiration, DNA replication, and cell division, and increase the surface area of bacterial membrane.[22,79,80] Moreover, mechanisms vary with particle size, surface charge, and concentration, and may differ across bacterial species.[75,81,82] In this experiment, TEM analysis revealed the presence of spherical or irregular nanoparticles situated between collagen fibrils (Figure 1a and b). Despite the aggregation of mineralized products within the collagen fibrils, a considerable number of cerium oxide nanoparticles remained discernible under TEM (Figure 1d). These nanoparticles probably exhibit antibacterial mechanisms akin to cerium oxide nanoparticles synthesized using traditional methods such as co-precipitation, sol-gel method, microemulsion, hydrothermal/solvothermal method, and others.[79] These findings strongly indicate that this method shows great potential in providing a powerful disinfection effect for root canal therapy.

In addition to their antibacterial properties, the biocompatibility of metal oxide nanoparticles is a critical aspect that necessitates thorough investigation, particularly in biomedical applications.[83,84] Numerous in vitro studies have indicated that well-engineered metal oxide nanoparticles, such as cerium oxide, exhibit favorable biocompatibility with various cell

types.[85–87] In vivo studies, conducted in animal models, have further affirmed the biocompatibility of cerium oxide nanoparticles in specific applications, including assessments of organ toxicity, inflammation, and other physiological responses.[88,89]

However, the biocompatibility of metal oxide nanoparticles is a multifaceted topic, contingent upon factors such as the specific metal oxide, particle size, surface characteristics, concentration, and the biological context of application.[83,90] Future investigations should prioritize a comprehensive understanding of the in vivo effects of this approach on root canal disinfection and the biocompatibility of cerium oxide nanoparticles when they are employed in root canal therapy.

Conclusion

This study provides strong evidence supporting the efficacy of employing cerium nitrate and dextran for the extra- and intrafibrillar mineralization of demineralized dentin, and the occlusion of dentinal tubules and lateral roots canals. The resultant modified dentin surface exhibits outstanding antibacterial properties. Consequently, this study introduces a novel and promising alternative strategy for endodontic infection control.

Acknowledgment

This work was supported by the National Natural Science Foundation of China (No. 81970982), Natural Scientific Research Fund of the Zhejiang Province, China (No. LGF20H140009) and Fujian Provincial Engineering Research Center of Oral Biomaterial, School and Hospital of Stomatology, Fujian Medical University (Grant No. 2023GC-A02). We thank Xiaomin Zhang, Xiaohuan Zhao and Nianhang Rong in the Analysis Center of Agrobiology and Environmental Sciences, Faculty of Agriculture, Life and Environment Sciences, Zhejiang University. We thank Zhemin Wu in the Center of Electron Microscopy, Zhejiang University, China, for technical assistance with STEM. We also thank Xiaoli Hong from the Core Facilities, Zhejiang University School of Medicine for the technical support.

Disclosure

The authors declare that they have no potential conflicts of interest with respect to the authorship and/or publication of this article.

References

1. Eleazer PD. *Glossary of endodontic terms*. American Association of Endodontists; 2003.
2. Siqueira JF. Microbial causes of endodontic flare-ups. *Int Endod J*. 2003;36(7):453–463. doi:10.1046/j.1365-2591.2003.00671.x
3. Waltimo T, Trope M, Haapasalo M, Orstavik D. Clinical efficacy of treatment procedures in endodontic infection control and one year follow-up of periapical healing. *J Endod*. 2005;31(12):863–866. doi:10.1097/01.don.0000164856.27920.85
4. Pedullà E, Abiad RS, Conte G, La Rosa GRM, Rapisarda E, Neelakantan P. Root fillings with a matched-taper single cone and two calcium silicate-based sealers: an analysis of voids using micro-computed tomography. *Clin Oral Investig*. 2020;24(12):4487–4492. doi:10.1007/s00784-020-03313-5
5. Wu MK, Wesselink PR. Efficacy of three techniques in cleaning the apical portion of curved root canals. *Oral Surg, Oral Med Oral Pathol Oral Radiol Endod*. 1995;79(4):492–496. doi:10.1016/s1079-2104(05)80134-9
6. Metzger Z, Teperovich E, Cohen R, Zary R, Paqué F, Hülsmann M. The self-adjusting file (SAF). Part 3: removal of debris and smear layer-A scanning electron microscope study. *J Endod*. 2010;36(4):697–702. doi:10.1016/j.joen.2009.12.037
7. Jr JFS. Aetiology of root canal treatment failure: why well-treated teeth can fail. *Int Endod J*. 2001;34(1):1–10. doi:10.1046/j.1365-2591.2001.00396.x
8. Persoon IF, Ozok AR. Definitions and Epidemiology of Endodontic Infections. *Curr Oral Health Rep*. 2017;4(4):278–285. doi:10.1007/s40496-017-0161-z
9. Gergely JM, DiFiore PM. Intracanal medication in endodontic treatment: a survey of endodontic programs. *Gen Dent*. 1993;41(4):328–331.
10. Kumar A, Tamanna S, Iftekhar H. Intracanal medicaments - Their use in modern endodontics: a narrative review. *J Oral Res Rev*. 2019;11(2):94–99. doi:10.4103/jorr.jorr_3_19
11. Ng YL, Mann V, Gulabivala K. A prospective study of the factors affecting outcomes of nonsurgical root canal treatment: part 1: periapical health. *Int Endod J*. 2011;44(7):583–609. doi:10.1111/j.1365-2591.2011.01872.x
12. Gilbert B, Luebke RG, Jeansonne BG, Henderson JA. Calcium hydroxide in endodontics: a review. *J La Dent Assoc*. 1981;39(1):12–15.
13. Plutzer B, Zilm P, Ratnayake J, Cathro P. Comparative efficacy of endodontic medicaments and sodium hypochlorite against Enterococcus faecalis biofilms. *Aust Dent J*. 2018;63(2):208–216. doi:10.1111/adj.12580
14. Mohammadi Z, Dummer PM. Properties and applications of calcium hydroxide in endodontics and dental traumatology. *Int Endod J*. 2011;44(8):697–730. doi:10.1111/j.1365-2591.2011.01886.x
15. Haapasalo M, Orstavik D. In vitro infection and disinfection of dentinal tubules. *J Dent Res*. 1987;66(8):1375–1379. doi:10.1177/00220345870660081801

16. Wong J, Manoil D, Nasman P, Belibasakis GN, Neelakantan P. Microbiological Aspects of Root Canal Infections and Disinfection Strategies: an Update Review on the Current Knowledge and Challenges. *Front Oral Health*. 2021;2:672887. doi:10.3389/froh.2021.672887
17. Beyth N, Houri-Haddad Y, Domb A, Khan W, Hazan R. Alternative antimicrobial approach: nano-antimicrobial materials. *Evid Based Complement Alternat Med*. 2015;2015:246012. doi:10.1155/2015/246012
18. Sánchez-Sanhueza G, Alcántara-Dufeu R, Carrillo L, Mansilla H, Novoa C, Bello-Toledo H. Ex vivo Effect of Copper Sulfate on Enterococcus faecalis in Root Canals. *Int J Dermatol*. 2015;9:505–510. doi:10.4067/S0718-381X2015000300024
19. Evans M, Davies JK, Sundqvist G, Figdor D. Mechanisms involved in the resistance of Enterococcus faecalis to calcium hydroxide. *Int Endod J*. 2002;35(3):221–228. doi:10.1046/j.1365-2591.2002.00504.x
20. Singh KR, Nayak V, Sarkar T, Singh RP. Cerium oxide nanoparticles: properties, biosynthesis and biomedical application. *RSC Adv*. 2020;10 (45):27194–27214. doi:10.1039/d0ra04736h
21. Farias IAP, Dos Santos CCL, Sampaio FC. Antimicrobial Activity of Cerium Oxide Nanoparticles on Opportunistic Microorganisms: a Systematic Review. *Biomed Res Int*. 2018;2018:1923606. doi:10.1155/2018/1923606
22. Zhang M, Zhang C, Zhai X, Luo F, Du Y, Yan C. Antibacterial mechanism and activity of cerium oxide nanoparticles. *Sci China Mater*. 2019;62 (11):1727–1739. doi:10.1007/s40843-019-9471-7
23. Kargozar S, Baino F, Hoseini SJ, et al. Biomedical applications of nanoceria: new roles for an old player. *Nanomedicine (Lond)*. 2018;13 (23):3051–3069. doi:10.2217/nnm-2018-0189
24. Nudelman F, Pieterse K, George A, et al. The role of collagen in bone apatite formation in the presence of hydroxyapatite nucleation inhibitors. *Nat Mater*. 2010;9(12):1004–1009. doi:10.1038/nmat2875
25. Toroian D, Lim JE, Price PA. The size exclusion characteristics of type I collagen: implications for the role of noncollagenous bone constituents in mineralization. *J Biol Chem*. 2007;282(31):22437–22447. doi:10.1074/jbc.M700591200
26. Zhou Z, Li J, Wang Z, et al. In-Depth Occlusion of Dentinal Tubules and Rapid Remineralization of Demineralized Dentin Induced by Polyelectrolyte-Calcium Complexes. *Adv Healthc Mater*. 2023:e2300100. doi:10.1002/adhm.202300100
27. Kung JC, Wang WH, Chiang YC, et al. The Antibacterial and Remineralization Effect of Silver-Containing Mesoporous Bioactive Glass Sealing and Er-YAG Laser on Dentinal Tubules Treated in a Streptococcus mutans Cultivated Environment. *Pharmaceuticals (Basel)*. 2021;14(11):56.
28. Zhou Z, Zhang L, Li J, Shi Y, Fu B. Polyelectrolyte-calcium Complexes as a Pre-precursor Induce Biomimetic Mineralization of Collagen. *Nanoscale*. 2021;13(2):953–967. doi:10.1039/d0nr05640e
29. Yared G. Canal preparation using only one Ni-Ti rotary instrument: preliminary observations. *Int Endod J*. 2008;41(4):339–344. doi:10.1111/j.1365-2591.2007.01351.x
30. Chen J, Zhao Q, Peng J, Yang X, Yu D, Zhao W. Antibacterial and mechanical properties of reduced graphene-silver nanoparticle nanocomposite modified glass ionomer cements. *J Dent*. 2020;96:103332. doi:10.1016/j.jdent.2020.103332
31. Paz L. Image analysis software based on color segmentation for characterization of viability and physiological activity of biofilms. *Appl Environ Microbiol*. 2009;75(6):1734–1739. doi:10.1128/AEM.02000-08
32. Perez JM, Asati A, Nath S, Kaittanis C. Synthesis of biocompatible dextran-coated nanoceria with pH-dependent antioxidant properties. *Small*. 2008;4(5):552–556. doi:10.1002/smll.200700824
33. Liao J, Meng Y, Zhai J, et al. Physicochemical, pharmacologic, and in vitro cellular effects of loading collagen membranes with zoledronic acid. *Int J Oral Maxillofac Implants*. 2013;28(4):1027–1036. doi:10.11607/jomi.3030
34. Song Q, Jiao K, Tonggu L, et al. Contribution of biomimetic collagen-ligand interaction to intrafibrillar mineralization. *Sci Adv*. 2019;5(3): eaav9075. doi:10.1126/sciadv.aav9075
35. Teng M, Luo L, Yang X. Synthesis of mesoporous Ce1xZrxO2 (x=0.20.5) and catalytic properties of CuO based catalysts. *Micropor Mesopor Mat*. 2009;119(1–3):158–164. doi:10.1016/j.micromeso.2008.10.019
36. Chen Y, Lu J. Facile fabrication of porous hollow CeO2 microspheres using polystyrene spheres as templates. *J Porous Mat*. 2012;19(3):289–294. doi:10.1007/s10934-011-9474-9
37. Wang R, Stanley T, Yao X, Liu H, Wang Y. Collagen stabilization by natural cross-linkers: a qualitative and quantitative FTIR study on ultra-thin dentin collagen model. *Dent Mater J*. 2022;41(3):440–450. doi:10.4012/dmj.2021-247
38. Akgun OM, Bayari SH, Ide S, Polat GG, Kalkhoran IO. Micro- and nanoscale structures of mesiodens dentin: combined study of FTIR and SAXS/WAXS techniques. *Microsc Res Tech*. 2015;78(1):52–58. doi:10.1002/jemt.22444
39. Chong BS, Pitt Ford TR. The role of intracanal medication in root canal treatment. *Int Endod J*. 1992;25(2):97–106. doi:10.1111/j.1365-2591.1992.tb00743.x
40. Prada I, Mico-Munoz P, Giner-Lluesma T, Mico-Martinez P, Collado-Castellano N, Manzano-Saiz A. Influence of microbiology on endodontic failure. Literature review. *Med Oral Patol Oral Cir Bucal*. 2019;24(3):e364–e372. doi:10.4317/medoral.22907
41. Raura N, Garg A, Arora A, Roma M. Nanoparticle technology and its implications in endodontics: a review. *Biomater Res*. 2020;24(1):21. doi:10.1186/s40824-020-00198-z
42. Stubbing J, Brown J, Price GJ. Sonochemical production of nanoparticle metal oxides for potential use in dentistry. *Ultrason Sonochem*. 2017;35(Pt B):646–654. doi:10.1016/j.ultsonch.2016.04.036
43. Louwakul P, Saelo A, Khemaleelakul S. Efficacy of calcium oxide and calcium hydroxide nanoparticles on the elimination of Enterococcus faecalis in human root dentin. *Clin Oral Investig*. 2017;21(3):865–871. doi:10.1007/s00784-016-1836-x
44. Afkhami F, Nasri S, Valizadeh S. Bacterial leakage assessment in root canals sealed with AH Plus sealer modified with silver nanoparticles. *BMC Oral Health*. 2021;21(1):577. doi:10.1186/s12903-021-01924-2
45. Brosco VH, Bernardineli N, Torres SA, et al. Bacterial leakage in obturated root canals-part 2: a comparative histologic and microbiologic analyses. *Oral Surg, Oral Med Oral Pathol Oral Radiol Endod*. 2010;109(5):788–794. doi:10.1016/j.tripleo.2009.11.036
46. Niu LN, Jee SE, Jiao K, et al. Collagen intrafibrillar mineralization as a result of the balance between osmotic equilibrium and electroneutrality. *Nat Mater*. 2017;16(3):370–378. doi:10.1038/nmat4789
47. Wang Z, Ouyang Y, Wu Z, et al. A novel fluorescent adhesive-assisted biomimetic mineralization. *Nanoscale*. 2018;10(40):18980–18987. doi:10.1039/c8nr02078g
48. Danesi PR. Studies on the Hydrolysis of Metal Ions. *Acta Chem Scand*. 1967;21(1):10.
49. Mesmer R, Baes C. Review of Hydrolysis Behavior of Ions in Aqueous Solutions. *MRS Online Proc Lib*. 1990;180:85–96.

50. Nanda HS. Surface modification of promising cerium oxide nanoparticles for nanomedicine applications. *RSC Adv*. 2016;6(113):111889–111894. doi:10.20944/preprints201608.0112.v1
51. Karakoti A, Monteiro-Riviere N, Aggarwal R, et al. Nanoceria as antioxidant: synthesis and biomedical applications. *Jom*. 2008;60:33–37. doi:10.1007/s11837-008-0029-8
52. Zhou Y, Liu K, Zhang H. Biomimetic Mineralization: from Microscopic to Macroscopic Materials and Their Biomedical Applications. *ACS Appl Bio Mater*. 2023. doi:10.1021/acsabm.3c00109
53. Oosterlaken BM, Vena MP, de With G. In vitro mineralization of collagen. *Adv Mater*. 2021;33(16):2004418. doi:10.1002/adma.202004418
54. Díaz-Montes E. Dextran: sources, structures, and properties. *Polysaccharides*. 2021;2(3):554–565. doi:10.3390/polysaccharides2030033
55. Ferreira MPA, Talman V, Torrieri G, et al. Dual-Drug Delivery Using Dextran-Functionalized Nanoparticles Targeting Cardiac Fibroblasts for Cellular Reprogramming. *Adv Funct Mater*. 2018;28:1705134. doi:10.1002/adfm.201705134
56. Arcot P, Kim D-S, Pak D, Sim S. Rheology and gelation of water-insoluble dextran from Leuconostoc mesenteroides NRRL B-523. *Carbohyd Polym*. 2003;53:459–468. doi:10.1016/S0144-8617(03)00140-1
57. Wang Y, Liu J, Shi T, et al. Synthesis, characterization and mechanism of porous spherical nesquehonite by CO2 biomimetic mineralization. *Adv Powder Technol*. 2022;33(12):103856. doi:10.1016/j.apt.2022.103856
58. Ju X, Šmíd B, Johánek V, et al. Investigation of dextran adsorption on polycrystalline cerium oxide surfaces. *Appl Surf Sci*. 2020;544:148890. doi:10.1016/j.apsusc.2020.148890
59. Dai L, Douglas EP, Gower LB. Compositional analysis of a polymer-induced liquid-precursor (PILP) amorphous CaCO3 phase. *J Non-Cryst Solids*. 2008;354(17):1845–1854. doi:10.1016/j.jnoncrysol.2007.10.022
60. Lotsari A, Rajasekharan AK, Halvarsson M, Andersson M. Transformation of amorphous calcium phosphate to bone-like apatite. *Nat Commun*. 2018;9(1):4170. doi:10.1038/s41467-018-06570-x
61. Perez RA, Ginebra MP. Injectable collagen/α-tricalcium phosphate cement: collagen-mineral phase interactions and cell response. *J Mater Sci Mater Med*. 2013;24(2):381–393. doi:10.1007/s10856-012-4799-8
62. Nyoka M, Choonara YE, Kumar P, Kondiah PP, Pillay V. Synthesis of cerium oxide nanoparticles using various methods: implications for biomedical applications. *Nanomaterials*. 2020;10(2):242. doi:10.3390/nano10020242
63. Deshpande S, Patil S, Kuchibhatla SV, Seal S. Size dependency variation in lattice parameter and valency states in nanocrystalline cerium oxide. *Appl Phys Lett*. 2005;87(13):133113. doi:10.1063/1.2061873
64. Baalousha M, Le Coustumer P, Jones I, Lead J. Characterisation of structural and surface speciation of representative commercially available cerium oxide nanoparticles. *Environ Chem*. 2010;7(4):377–385. doi:10.1071/EN10003
65. Kenneth R, Aniruddha K, Alastair C. Exploring the properties and applications of nanoceria: is there still plenty of room at the bottom? *Environ Sci-Nano*. 2014;1(5):390–405. doi:10.1039/C4EN00079J
66. van der Sluis LW, Wu MK, Wesselink PR. An evaluation of the quality of root fillings in mandibular incisors and maxillary and mandibular canines using different methodologies. *J Dent*. 2005;33(8):683–688. doi:10.1016/j.jdent.2005.01.007
67. Li C, Lu D, Deng J, Zhang X, Yang P. Amyloid-Like Rapid Surface Modification for Antifouling and In-Depth Remineralization of Dentine Tubules to Treat Dental Hypersensitivity. *Adv Mater*. 2019;31(46):e1903973. doi:10.1002/adma.201903973
68. Wen Y, Wang J, Luo J, Yang J. Remineralization of dentine tubules induced by phosphate-terminated PAMAM dendrimers. *Heliyon*. 2020;6(12):e05886. doi:10.1016/j.heliyon.2020.e05886
69. Toledano M, Vallecillo-Rivas M, Aguilera FS, Osorio MT, Osorio E, Osorio R. Polymeric zinc-doped nanoparticles for high performance in restorative dentistry. *J Dent*. 2021;107:103616. doi:10.1016/j.jdent.2021.103616
70. Melo MA, Cheng L, Weir MD, Hsia RC, Rodrigues LK, Xu HH. Novel dental adhesive containing antibacterial agents and calcium phosphate nanoparticles. *J Biomed Mater Res B Appl Biomater*. 2013;101(4):620–629. doi:10.1002/jbm.b.32864
71. Beveridge TJ, Graham LL. Surface layers of bacteria. *Microbiol Rev*. 1991;55(4):684–705. doi:10.1128/mr.55.4.684-705.1991
72. Qi M, Li W, Zheng X, Li X, Wang L. Cerium and Its Oxidant-Based Nanomaterials for Antibacterial Applications: a State-of-The-Art Review. *Front Mater*. 2020;7. doi:10.3389/fmats.2020.00213
73. Predoi D. Investigation of Spin Coating Cerium-Doped Hydroxyapatite Thin Films with Antifungal Properties. *Coatings*. 2021;11.
74. Li Y, Zhang W, Niu J, Chen Y. Mechanism of photogenerated reactive oxygen species and correlation with the antibacterial properties of engineered metal-oxide nanoparticles. *ACS Nano*. 2012;6(6):5164–5173. doi:10.1021/nn300934k
75. Alpaslan E, Geilich BM, Yazici H, Webster TJ. pH-Controlled Cerium Oxide Nanoparticle Inhibition of Both Gram-Positive and Gram-Negative Bacteria Growth. *Sci Rep*. 2017;7:45859. doi:10.1038/srep45859
76. Wang L, He H, Yu Y, et al. Morphology-dependent bactericidal activities of Ag/CeO2 catalysts against Escherichia coli. *J Inorg Biochem*. 2014;135:45–53. doi:10.1016/j.jinorgbio.2014.02.016
77. Arumugam A, Karthikeyan C, Haja Hameed AS, Gopinath K, Gowri S, Karthika V. Synthesis of cerium oxide nanoparticles using Gloriosa superba L. leaf extract and their structural, optical and antibacterial properties. *Mater Sci Eng C Mater Biol Appl*. 2015;49:408–415. doi:10.1016/j.msec.2015.01.042
78. Tong GX, Du FF, Liang Y, et al. Polymorphous ZnO complex architectures: selective synthesis, mechanism, surface area and Zn-polar plane-codetermining antibacterial activity. *J Mater Chem B*. 2013;1(4):454–463. doi:10.1039/c2tb00132b
79. Nadeem M, Khan R, Afridi K, et al. Green Synthesis of Cerium Oxide Nanoparticles (CeO(2) NPs) and Their Antimicrobial Applications: a Review. *Int J Nanomed*. 2020;15:5951–5961. doi:10.2147/IJN.S255784
80. Barker E, Shepherd J, Asencio IO. The Use of Cerium Compounds as Antimicrobials for Biomedical Applications. *Molecules*. 2022;27(9):5655.
81. Pelletier DA, Suresh AK, Holton GA, et al. Effects of engineered cerium oxide nanoparticles on bacterial growth and viability. *Appl Environ Microbiol*. 2010;76(24):7981–7989. doi:10.1128/aem.00650-10
82. Kuang Y, He X, Zhang Z, et al. Comparison study on the antibacterial activity of nano- or bulk-cerium oxide. *J Nanosci Nanotechnol*. 2011;11(5):4103–4108. doi:10.1166/jnn.2011.3858
83. Wang Z, Tang M. Research progress on toxicity, function, and mechanism of metal oxide nanoparticles on vascular endothelial cells. *J Appl Toxicol*. 2021;41(5):683–700. doi:10.1002/jat.4121
84. Humaira B, Shakir HA, et al. Biosynthesized Cerium Oxide Nanoparticles CeO(2)NPs: recent Progress and Medical Applications. *Curr Pharm Biotechnol*. 2023;24(6):766–779. doi:10.2174/1389201023666220821161737

85. Ma X, Cheng Y, Jian H, et al. Hollow, Rough, and Nitric Oxide-Releasing Cerium Oxide Nanoparticles for Promoting Multiple Stages of Wound Healing. *Adv Healthc Mater*. 2019;8(16):e1900256. doi:10.1002/adhm.201900256
86. Vedhanayagam M, Kumar AS, Nair BU, Sreeram KJ. Dendrimer-Functionalized Metal Oxide Nanoparticle-Mediated Self-Assembled Collagen Scaffold for Skin Regenerative Application: function of Metal in Metal Oxides. *Appl Biochem Biotechnol*. 2022;194(1):266–290. doi:10.1007/s12010-021-03764-w
87. Xie W, Guo Z, Gao F, et al. Shape-, size- and structure-controlled synthesis and biocompatibility of iron oxide nanoparticles for magnetic theranostics. *Theranostics*. 2018;8(12):3284–3307. doi:10.7150/thno.25220
88. Cordelli E, Keller J, Eleuteri P, et al. No genotoxicity in rat blood cells upon 3- or 6-month inhalation exposure to CeO2 or BaSO4 nanomaterials. *Mutagenesis*. 2017;32(1):13–22. doi:10.1093/mutage/gew005
89. Goujon G, Baldim V, Roques C, et al. Antioxidant Activity and Toxicity Study of Cerium Oxide Nanoparticles Stabilized with Innovative Functional Copolymers. *Adv Healthc Mater*. 2021;10(11):e2100059. doi:10.1002/adhm.202100059
90. Raghunath A, Perumal E. Metal oxide nanoparticles as antimicrobial agents: a promise for the future. *Int J Antimicrob Agents*. 2017;49(2):137–152. doi:10.1016/j.ijantimicag.2016.11.011